Downstream control on the stability of river bifurcations

Lorenzo Durante,[1] Michele Bolla Pittaluga,[1] Gaetano Porcile,[1,2] Nicoletta Tambroni[1]

[1]Department of Civil, Chemical and Environmental Engineering, University of Genova, Genova, Italy.
[2]Coastal and Continental Morphodynamics Laboratory, University of Caen Normandy, Caen, France.

Key Points:

- A new formulation for the stability of river bifurcations based on energy balance at the node is proposed.
- The bifurcation stability has been found to increase as the branches length decreases.
- Despite the presence of asymmetry at the node, the less-favoured side can become dominant under certain conditions.

Corresponding author: Lorenzo Durante, `lorenzo.durante@edu.unige.it`

Abstract

River bifurcations are prevalent features in both gravel-bed and sand-bed fluvial systems, including braiding networks, anabranches and deltas. Therefore, gaining insight into their morphological evolution is important to understand the impact they have on the adjoining environment. While previous investigations have primarily focused on the influence on bifurcation morphodynamics by upstream channels, recent research has highlighted the importance of downstream controls, like branches length or tidal forcing. In particular, in the case of rivers, current linear stability analyses for a simple bifurcation are unable to capture the stabilizing effect of branches length unless a confluence is added downstream. In this work, we introduce a novel theoretical model that effectively accounts for the effects of downstream branch length in a single bifurcation. To substantiate our findings, a series of fully 2D numerical simulations are carried out to test different branches lengths and other potential sources of asymmetries at the node, such as different widths of the downstream channels. Results from linear stability analysis show that bifurcation stability increases as the branches length decreases. These results are confirmed by the numerical simulations, which also show that, as the branch length tends to vanish, bifurcations are invariably stable. Finally, our results interestingly show that, while in general, when a source of asymmetry is present at the node, the hydraulically favoured branch dominates, there are scenarios in which the less-favoured side becomes dominant.

Plain Language Summary

This research looks at how rivers divide into multiple branches and how this process shapes the surrounding environment. While past studies mostly focused on factors upstream influencing these splits, recent research emphasizes the importance of downstream factors, such as branch length and tidal forces. The study introduces a new theoretical model to better understand how downstream branch length affects a single river split. We used computer simulations with different branch lengths and channel widths to test the model, discovering that shorter branch lengths result in more stable river splits. The theoretical model is also adapted to account for different shapes commonly found in nature, revealing results that are not always straightforward.

1 Introduction

Rivers have always covered a fundamental role in the evolution of humankind. Due to the high economic interest and risk associated to these areas, humans have always tried to control and modify these environments to sustain their activities. Noteworthy, this feature has become even more evident in the last decades due to an increase both of the intensity of the natural forcings (due to climate change, extreme events are becoming more frequent) and of the anthropogenic actions (e.g., the building of dams and other flow control structures in the upstream part of rivers).

However, even if extreme events require detailed analyses, the morphodynamic development of rivers, estuaries and deltas is commonly studied referring to the concept of a formative or effective forcing which represents the most frequent condition that these systems experience over time [*Wolman & Miller*, 1960; *Williams*, 1978]. This allows to estimate the long term river equilibrium configuration and predict if some perturbation of this state can permanently modify it, leading to erosional or depositional processes and to variations of the planar configuration [*Bolla Pittaluga et al.*, 2014; *Wilkerson & Parker*, 2011].

One crucial control unit in the evolution of rivers and deltas is the bifurcation, which governs both flow and sediment partitioning in downstream branches, thus, affecting downstream erosion or deposition [*Jerolmack*, 2009; *Tejedor et al.*, 2017; *Nienhuis et al.*, 2020]. A typical case where one bifurcate closes completely is the avulsions of meandering rivers

with chute cut-offs: the branch with the highest carrying capacity becomes the main channel, while the other, known as oxbow lake, remains isolated [*Seminara*, 2006; *Viero et al.*, 2018]. These phenomena have historically led to approach the problem of the stability

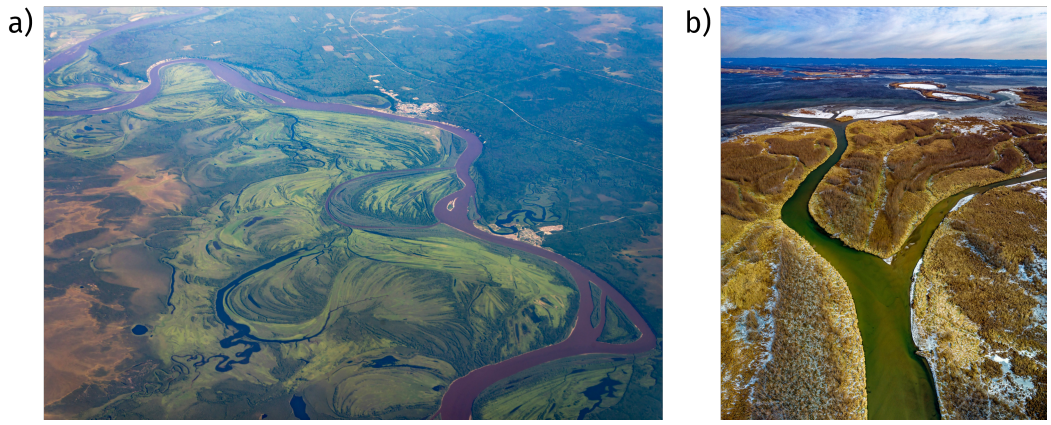

Figure 1. Example of natural bifurcations. a) Fast migrating meandering river in the Republic of Khakassia, Russia. (Photo by Denis Ovsyannikov: https://www.pexels.com/@denis-ovsyannikov-1411283/). b) River bifurcates debouching into a lake in Altura, US. (Photo by Tom Fisk: https://www.pexels.com/@tomfisk/).

of the bifurcations in terms of their upstream forcings in both gravel-bed and sand-bed fluvial systems. Early analytical works were proposed by *Wang et al.* [1995], who performed a 1D analysis, including an empirical nodal point condition at the bifurcation node to evaluate the partitioning in the branches. This condition turns out to depend on a parameter that is not related to the physics of the system but governs its evolution in time. Thus, *Bolla Pittaluga et al.* [2003] overcame this limit by introducing a two-cell model which accounts for the localized 2-D effects upstream of the bifurcation node in terms of sediment and flow division. Applying it to both gravel-bed and sand-bed rivers, *Bolla Pittaluga et al.* [2015] found that the stability is mainly dependent on the Shields parameter ϑ and on the aspect ratio ($\beta = \frac{W}{2D}$) of the upstream channel. However, also in this model, some empirical parameters need to be specified. Indeed, the critical value of the aspect ratio above which a bifurcation becomes unstable, is found to be linearly dependent on the length of the two upstream cells α and on the 'Talmon' parameter r accounting for the contribution of the transversal bed slope on the sediment transport [*Talmon et al.*, 1995]. Common values of the parameter r range between 0.3 and 1 [*Ikeda et al.*, 1981], while the experimental calibration of the parameter α provides values from 1 to 6 [*Bolla Pittaluga et al.*, 2003; *Bertoldi and Tubino*, 2007].

This notwithstanding, the simple two-cell model has proven to be able to adequately reproduce the main mechanism governing the morphodynamic evolution of a river bifurcation. Consequently, efforts have been made to extend this model to account for some additional effects that were neglected in the original formulation. *Miori et al.* [2006] included channel width variations according to hydraulic geometry rules. *Bertoldi et al.* [2009] studied the effect of incoming migrating bars by integrating the bifurcation model with the model of *Colombini et al.* [1987], which provides the spatial structure and the temporal development of finite amplitude bars. *Kleinhans et al.* [2008] analysed the effect of the secondary flow due to an upstream meander bend on the bifurcation stability. Later *Redolfi et al.* [2019] studied the combined effect of upstream radius of curvature and slope advantage in the two branches. Recently, *Ragno et al.* [2023] managed to examine the effect of sediment sorting on the unbalanced bifurcations.

However, these studies predominantly focused on the upstream forcings, without accounting for the potential feedback mechanisms arising from the downstream ones. *Salter et al.* [2018], for instance, investigated the consequences of prograding branches finding an oscillating behaviour attributed to the restorative feedback arising from the gentler slope in the longer branch. The length of the branches thus emerges as a determining factor for bifurcation stability. Recently, *Ragno et al.* [2021] applied the two-cell model to a bifurcation-confluence loop by introducing a momentum balance model for the downstream junction. This revealed the system being more stable as the confluence influence increases (i.e. decreasing the branch lengths). Furthermore, the distance of the bifurcation node from the downstream boundary has once again proven to be crucial when incorporating the two-cell model with downstream effects, such as the tidal forcings [*Ragno et al.*, 2020; *Iwantoro et al.*, 2020]. This set its basis on the observations that, even in micro-tidal environments, tides exert a profound influence on distributary hydrodynamics throughout both high and low fluvial discharge regimes [*Leonardi et al.*, 2015].

The considerations outlined above lead us to question whether the original two-cell model of *Bolla Pittaluga et al.* [2003] can be reliably applied in scenarios where downstream effects are not negligible. It is important to note that the model operates under the assumption that the free surface elevations remain constant at the bifurcation node regardless of flow conditions. However, this condition may no longer hold when the downstream conditions influence the bifurcation, as is the case with short branch lengths. Since any disturbance of the flow could potentially trigger a destabilization of the system, we relax the constraint of constant water elevations at the node, incorporating an energy balance condition between the upstream and the downstream branches. This approach allows for flow asymmetries to directly impact the morphological equilibrium of river bifurcations. The system of equations arising from the new formulation is tackled with linear stability analysis, allowing us to account for the length of the branches on the stability and equilibrium configurations of the river network. To validate the theoretical findings, numerical simulations are conducted, yielding results consistent with our analytical framework. In the current study, we formulate the model in its most comprehensive form accounting also for other possible sources of asymmetries at the node. Given that natural river bifurcations typically exhibit limited symmetry, we analyse the effect of various asymmetries individually to gain insights into their impact on equilibrium configurations.

The subsequent Section will provide a detailed explanation of the analytical procedure employed in this study. Section 3 will be dedicated to presenting and discussing the theoretical and numerical findings obtained for symmetric scenarios. In section 4, the asymmetries in the system are analyzed independently to discern their respective impacts on the equilibrium configuration of bifurcations. Finally, in Section 5, we will summarize our key observations and insights.

2 Formulation of the analytical model

As previously discussed, the equilibrium of bifurcations is predominantly influenced by the flow and sediment division at the node. Given the complexity of factors governing the system's evolution, it is necessary to simplify the problem for analytical handling. The bifurcation is then idealized as an upstream rectangular channel a, which bifurcates into two branches, channels b and c (as depicted in Figure 2), respectively. No parameter variability is included along any channel, thus, they all have constant widths (W_a^*, W_b^*, W_c^*), even though the two downstream branches could have different lengths (l_b^*, l_c^*). Furthermore, it is assumed that the system evolves primarily due to formative forcing, therefore, steady uniform flow is established in the channels through a constant discharge upstream Q_a^* and a fixed water level elevation at the two downstream ends (h_b^{*L}, h_c^{*L}). For every channel ($i = a, b, c$) the steady and uniform flow is described by the

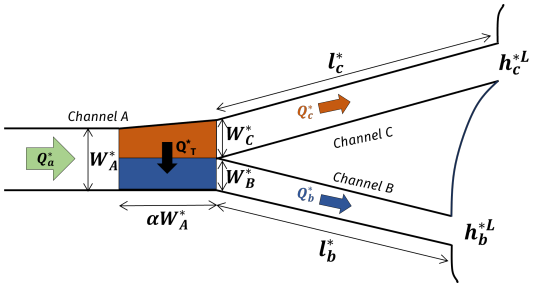

Figure 2. Representative sketch of theoretical river bifurcations. Sketch of the two-cell model of *Bolla Pittaluga et al.* [2003] extended to account for uneven branch widths and lengths.

Chezy relation:

$$Q_i^* = W_i^* D_i^* C_i \sqrt{g s_i D_i^*} \tag{1}$$

where D_i^* is the uniform flow depth in the channel i, g is the gravitational acceleration, C_i is the Chezy coefficient and s_i is the longitudinal bed slope.

Constant sediment discharge is provided in equilibrium with the flow conditions upstream. It is computed in general terms by the following relation:

$$\phi = \frac{q_{is}^*}{\sqrt{\frac{\rho_s - \rho}{\rho} g d_s^{*3}}} = n(D_i^*)(\vartheta_i - \vartheta_{cr})^m. \tag{2}$$

where q_{is}^* is the dimensional volumetric sediment flux per unit width of the i channel, d_s^* is the mean diameter, ρ and ρ_s are the density of water and sediment respectively, ϑ_{cr} is the threshold value for sediment mobilization and the coefficients n and m depend on the sediment transport closure relation. Finally, ϑ_i is the value of the Shields parameter associated with the uniform flow in the i^{th} channel:

$$\vartheta_i = \frac{q_i^{*2}}{\frac{\rho_s - \rho}{\rho} g d_s^* C_i^2 D_i^{*2}}. \tag{3}$$

being q_i^{*2} the flow discharge per unit width.

The model accounts for the two-dimensional effects at the node considering a transverse exchange of flow and sediment between the two upstream cells through the following nodal point condition:

$$q_{Ts}^* = q_{as}^* \left[\frac{Q_T^* D_a^*}{Q_a^* \alpha D_{abc}^*} - \frac{r}{\sqrt{\vartheta_a}} \frac{\partial \eta^*}{\partial y^*} \right]. \tag{4}$$

where q_{Ts}^* is the dimensional transverse solid discharge per unit width and Q_T^* is the total transverse flow discharge, $\partial \eta^* / \partial y^*$ is the transverse bed slope calculated as incremental ratio between the difference in bed elevations of the inlet of channels b and c and the semi-width of the upstream channel, and D_{abc}^* is the average water depth at the node. The latter can be safely assumed equal to D_a^*, such that $D_a^*/D_{abc}^* \simeq 1$. The parameter α is the length of the two cells scaled with the upstream channel width W_a^*; from experimental observations, it attains values between 1 and 3. The constant r in equation (4) has been experimentally determined and it ranges between 0.3 and 1 [*Ikeda et al.*, 1981; *Talmon et al.*, 1995].

To solve the problem, other five relations are required. Noteworthy, here we replace the conditions for water level constancy of *Bolla Pittaluga et al.* [2003] with an energy head E^* (i.e., the total energy per unit weight of flowing liquid above an horizontal datum) balance at the node:

1. Flow discharge balance:

$$q_a^* W_a^* = q_b^* W_b^* + q_c^* W_c^* \tag{5}$$

2. Solid discharge balance:

$$q_{as}^* W_a^* = q_{bs}^* W_b^* + q_{cs}^* W_c^* \tag{6}$$

3. Flow discharge balance applied to cell b:

$$q_a^* W_a^* \frac{W_b^*}{W_b^* + W_c^*} + q_T^* \alpha W_a^* = q_b^* W_b^* \tag{7}$$

4. Solid discharge balance applied to cell b:

$$q_{as}^* W_a^* \frac{W_b^*}{W_b^* + W_c^*} + q_{Ts}^* \alpha W_a^* = q_{bs}^* W_b^* \tag{8}$$

5. Energy head balance applied to cell b:

$$h_a^{*N} + \frac{q_a^{*2}}{2gD_a^{*2}} - \alpha W_a^* s_a = h_b^{*N} + (1+\xi)\frac{q_b^{*2}}{2gD_b^{*2}} \tag{9}$$

6. Energy head balance applied to cell c:

$$h_a^{*N} + \frac{q_a^{*2}}{2gD_a^{*2}} - \alpha W_a^* s_a = h_c^{*N} + (1+\xi)\frac{q_c^{*2}}{2gD_c^{*2}} \tag{10}$$

where ξ is a energy loss coefficient which has been introduced to account for possible localised fluid's energy dissipation at the node, in analogy with what it is commonly assumed in the case of pipe flows. Finally h_i^{*N} indicates the free surface elevation of the i^{th} channel at the node. Recalling the assumption of uniform flow in the branches, it is possible to rewrite h_i^{*N} as a function of the imposed level at the downstream end: $h_i^{*N} = h_i^{*L} + s_i l_i^*$.

The aforementioned equations can be made dimensionless, scaling the variables with the typical physical characteristics of the channel a as follows:

$$(D_i, h_i^N, h_i^L) = \frac{(D_i^*, h_i^{*N}, h_i^{*L})}{D_a^*}. \tag{11}$$

$$(q_{is}, q_{Ts}) = \frac{(q_{is}^*, q_{Ts}^*)}{q_{as}^*}, \quad (q_i, q_T) = \frac{(q_i^*, q_T^*)}{q_a^*}. \tag{12}$$

$$L_i = \frac{l_i^* s_a}{D_a^*}. \tag{13}$$

Note that, the branches' lengths are scaled with the backwater length (D_a^*/s_a).

After some manipulations, the governing equations (5)-(10) and the nodal point condition (4) can thus be rewritten in a dimensionless form as:

1. Flow discharge balance:

$$q_b r_b + q_c(r_a - r_b) = 1 \tag{14}$$

2. Solid discharge balance:

$$q_{bs} r_b + q_{cs}(r_a - r_b) = 1 \tag{15}$$

3. Energy balance:

$$\Delta h^L + L_b \left[\frac{q_b^2 C_a^2}{D_b^3 C_b^2} - \frac{q_c^2 C_a^2}{D_c^3 C_c^2} \gamma_L \right] + \frac{Fr^2}{2}(1+\xi)\left[\frac{q_b^2}{D_b^2} - \frac{q_c^2}{D_c^2} \right] = 0 \tag{16}$$

4. Nodal condition:

$$q_{bs} = q_b - \frac{\alpha r}{\beta\sqrt{\theta_a}} \frac{1}{r_a r_b} \left[(h_b^N - h_c^N) - (D_b - D_c) \right] . \tag{17}$$

Note that the above equations include the dependence on classical parameters of bifurcation theory as proposed by *Bolla Pittaluga et al.* [2003]. These parameters are the aspect ratio, β, defined as

$$\beta = \frac{W_a^*}{2D_a^*}, \tag{18}$$

and the Shields parameter of the upstream channel θ_a. Additionally, the Froude Number of the upstream channel, $Fr = q_a^*/\sqrt{gD_a^{*3}}$, and the following dimensionless parameters, accounting for possible asymmetries in the system, appear:

(a) Branch width ratios: $r_b = \frac{W_b^*}{W_a^*}$, $r_c = \frac{W_c^*}{W_a^*}$

(b) Downstream enlargement: $r_a = \frac{W_b^* + W_c^*}{W_a^*} = r_b + r_c$

(c) Length ratio: $\gamma_L = \frac{L_c}{L_b}$

(d) Downstream level asymmetry: $\Delta h^L = h_b^L - h_c^L$.

Finally, it is noteworthy that, the specific load balance equation (16) derives from equating the second members of equations (9) and (10), and that, in the nodal point condition (17), the transverse sediment and flow discharges have been derived from the previous (7) and (8) conditions.

2.1 Linear Stability Analysis

Through a linearization procedure, it is possible to solve numerically the system of equations (14)-(17), in terms of the four unknowns [q_b, q_c, D_b, D_c] (or [s_b, s_c, D_b, D_c]), finding the threshold conditions for the appearance of multiple equilibrium configurations. A perturbative approach is, thus, employed whereby every unknown f ([q_b, q_c, D_b, D_c]) is expanded in terms of a small parameter δ as follows:

$$f = f_0 + \delta f_1 + \mathcal{O}(\delta^2) \ , \tag{19}$$

where f_0 represents the basic state, namely, the uniform flow conditions. Similar expansions to (19) hold for any other variable g depending on the unknowns of the problem, where g_1 derives from a Taylor expansion around the basic state, in the form $g_1 = \frac{dg}{d\delta}\Big|_{\delta=0}$.

Substituting the expansions in the equations (14)-(17), it is possible to solve the system at each order of approximation. At the leading order, a set of non-linear algebraic equations in terms of the basic state variable arises, that can be solved with a central finite-difference solver. Differently from the classical case of equal length and width of the branches b and c, in the general case of different geometrical characteristics of the two downstream branches, at the leading order, $\mathcal{O}(\delta^0)$, we do not find a symmetrical water and sediment discharge distribution between them, but rather we find multiple equilibrium configurations. The order $\mathcal{O}(\delta)$ problem, consists of an homogeneous linear system of equations that has the form:

$$\begin{bmatrix} A_{11} & A_{12} & A_{13} & A_{14} \\ A_{21} & A_{22} & A_{23} & A_{24} \\ A_{31} & A_{32} & A_{33} & A_{34} \\ A_{41} & A_{42} & A_{43} & A_{44} \end{bmatrix} \begin{bmatrix} q_{b1} \\ q_{c1} \\ D_{b1} \\ D_{c1} \end{bmatrix} = \begin{bmatrix} 0 \\ 0 \\ 0 \\ 0 \end{bmatrix} \tag{20}$$

with the A_{ij} coefficients reported in Appendix A: . The sign of the eigenvalues associated with the matrix of the coefficient of the above linear system of algebraic equations allows to determine if the multiple equilibrium configurations found at the leading order are stable or not.

3 The case of Symmetrical Bifurcations

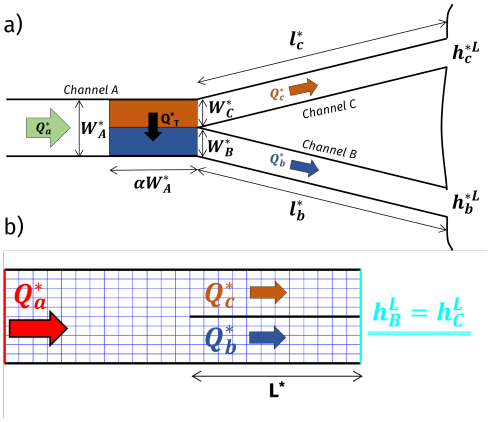

Figure 3. Representative sketches of theoretical and numerical river bifurcations. a) Sketch of the symmetrical two-cell model of *Bolla Pittaluga et al.* [2003]. b) Synthetic sketch of the numerical grid of a symmetrical river bifurcation.

3.1 Linear Stability Analysis

To understand the basic mechanisms underlying bifurcation stability, let us first consider the case of a completely symmetrical bifurcation (as depicted in Figure 3a) (i.e. r_a=1, r_b=0.5, γ_L=1, Δh^L=0 and ξ=0). In this case the solution at the leading order of the perturbation approach (Section 2.1) is the trivial solution, where the flow is equally partitioned in the downstream branches and there is no transversal exchange between the cells. At the first-order approximation, the flows and depths are anti-symmetric between b and c, therefore, the system (20) reduces to two equations, with unknowns associated to just one of the two downstream branches (e.g, D_b and q_b). Nontrivial solutions are found setting the determinant of the matrix of the coefficients equal to 0. The procedure allows for an algebraic relation for the critical aspect ratio β_{cr}, reading:

$$\beta_{cr} = \frac{4\alpha r}{\sqrt{\vartheta_a}} \frac{\left[2L_b + Fr^2 + L_b Fr^2 (2c_D + 1)\right]}{(L_b\gamma_1 + Fr^2\gamma_2)}, \tag{21}$$

with:

$$\gamma_1 = 2\left(\phi_\vartheta + \phi_n + c_D\right) - 3, \;\; \gamma_2 = -2\phi_\vartheta c_D + \phi_n - \frac{1}{2}. \tag{22}$$

and the coefficients c_D, ϕ_ϑ and ϕ_n defined as:

$$c_D = \frac{1}{C_0}\frac{\partial C_b}{\partial D_b}\bigg|_{D_0}, \;\; \phi_\vartheta = \frac{m\vartheta_a}{\vartheta_a - \vartheta_{cr}}, \;\; \phi_n = \frac{1}{n}\frac{\partial n}{\partial D_b}\bigg|_{D_0}. \tag{23}$$

They represent the sensitivity of the Chezy coefficient and of the dimensionless sediment transport rate to variations of water depth and Shields stress as similarly defined by *Redolfi et al.* [2019].

The aspect ratio β_{cr} represents the critical conditions for the stability of the symmetrical bifurcations: those with $\beta < \beta_{cr}$ (i.e., narrower upstream channels) are deemed stable, while, when $\beta > \beta_{cr}$ the symmetrical solution becomes unstable, leading to the dominance of one of the two branches.

For a clearer representation, let's consider the case where the roughness is defined with the Strickler relationship in an infinitely wide channel:

$$C_i = \frac{k_s^* D_i^{*1/6}}{\sqrt{g}} \ , \tag{24}$$

where k_s^* is the Gauckler-Strickler coefficient.

As far as the closure relationship for sediment transport is concerned, in the case of gravel-bed rivers, a relation of the type of *Meyer-Peter and Müller* [1948] might be used:

$$\phi_{MPM} = 8(\vartheta_a - \vartheta_{cr})^{1.5}, \tag{25}$$

leading to the following algebraic relation for β_{cr}:

$$\beta_{cr} = \frac{4}{3}\frac{\alpha r}{\sqrt{\vartheta_a}} \frac{(6L_b + 3Fr^2 + 4L_b Fr^2)}{\left[\frac{\vartheta_a}{\vartheta_a - \vartheta_{cr}}(3L_b - \frac{1}{2}Fr^2) - \frac{10}{3}L_b - Fr^2\right]}. \tag{26}$$

On the contrary, in the case of sand-bed rivers, as a fist approximation, the *Engelund and Hansen* [1967] relationship for the total sediment transport can be used:

$$\phi_{EH} = 0.05 C_i^2 \vartheta_i^{2.5}. \tag{27}$$

The corresponding relation for the critical aspect ratio β_{cr} takes the form:

$$\beta_{cr} = \frac{4}{3}\frac{\alpha r}{\sqrt{\vartheta_a}} \frac{(6L_b + 3Fr^2 + 4L_b Fr^2)}{(7/3L_b - 3/2Fr^2)}. \tag{28}$$

Noteworthy, setting $Fr = 0$ in (28) (i.e., not considering the kinetic head at the node), the solution coincides with that found by *Bolla Pittaluga et al.* [2015]:

$$\beta_{cr} = \frac{24}{7}\frac{\alpha r}{\sqrt{\vartheta_a}}. \tag{29}$$

Moreover, the two solutions reach almost the same values when the branches' lengths tend to infinity, meaning that the downstream conditions are not felt at the bifurcation node:

$$L_b \to \infty : \quad \beta_{cr} = \frac{24}{7}\frac{\alpha r}{\sqrt{\vartheta_a}}(1 + 2/3Fr^2). \tag{30}$$

3.2 Numerical Tests

The case of symmetrical bifurcations (i.e., where the branches have equal length and width) has also been tested with a systematic set of depth-averaged numerical simulations performed with the software suite Delft3D. The package Delft3D-FLOW solves the three-dimensional shallow water equations for incompressible fluid with a finite-difference scheme. It comprehends the exchange of sediment with the bed and, also, includes a morphological acceleration factor (*MorFac*) to speed up long-term morphological evolution *Lesser et al.* [2004].

The symmetrical bifurcation is represented as a fixed-bank, free-slip, rectangular channel a split by a thin dam into two branches b and c with equal length ($l_b^* = l_c^*$) and equal width ($W_b^* = W_c^* = W_a^*/2$), as sketched in Figure 3b. The overall length of the domain, L_{tot}^*, is a multiple of the backwater length L_{back}^* to avoid interferences at the inflow. The computational grid comprises 10 cells in the transversal direction, maintaining an aspect ratio equal to 1 (i.e., $\Delta x = \Delta y$) so that 5 transversal cells are employed in each downstream branch. With this design, the overall width remains constant throughout the domain without any loss of computational grid cells. A careful reader might notice that in this way the number of cells in the longitudinal direction depends not only on L_{tot}^*, but also on the width W_a^*, making the overall number of computational

317 **Table 1.** Summary of symmetrical numerical simulations.

ID	β	L	**ID**	β	L
$run01$	5	0.5	$run14$	16	1.5
$run02$	10	1	$run15$	20	0.1
$run03$	10	1.5	$run16$	20	0.2
$run04$	12	0.1	$run17$	20	0.3
$run05$	12	0.5	$run18$	25	0.1
$run06$	12	1.5	$run19$	25	0.2
$run07$	16	0.05	$run20$	33	0.05
$run08$	16	0.1	$run21$	33	0.1
$run09$	16	0.2	$run22$	33	0.2
$run10$	16	0.3	$run23$	41	0.05
$run11$	16	0.4	$run24$	41	0.1
$run12$	16	0.5	$run25$	41	0.5
$run13$	16	1			

315 cells case-dependent. Following the same reasoning, the computational time step was changed
316 depending on the grid size always obeying to the Courant–Frederichs–Levy criterion.

318 The investigation carried out in this study involves a systematic set of simulations,
319 wherein the channel width is varied to explore the impact of the main channel aspect
320 ratio β_a on the bifurcation stability, as summarized in Table 1. The stability of each con-
321 figuration is assessed by perturbing the bed profile of one branch with a cosine-shaped
322 deposit of amplitude $0.1D_a^*$. This perturbation ensures that the water depth at the bi-
323 furcation node and downstream boundary remains consistent with the previous equilib-
324 rium. As the simulation progresses, a step is observed in the perturbed branch at the
325 bifurcation node, while the other branch shows signs of incipient erosion. To track the
326 temporal evolution of the system, the discharge asymmetry ΔQ between the branches
327 is computed:

328 $$\Delta Q = \frac{Q_b^* - Q_c^*}{Q_a^*}. \tag{31}$$

341 In those cases when ΔQ approaches values close to 0, the bifurcation is stable, indicat-
342 ing equal partitioning of the flow. Conversely, when it reaches ± 1 one of the two branches
343 carries all the flow coming from the upstream channel a.

344 To maintain consistency with theoretical considerations and ease comparison be-
345 tween the different results, the slope s_a and the discharge per unit width q_a are kept con-
346 stant in every configuration, equal to $2{\times}10^{-4}$ and $0.44\ m^2/s$ respectively. This approach
347 ensures the establishment of a uniform flow depth D_a^* in equilibrium with the prescribed
348 inflow discharge, while maintaining a constant Shields number ($\vartheta_a = 0.15$) and a dimen-
349 sionless grains size ($d_s = d_s^*/D_a^*$) equal to 8.2×10^{-4} throughout all simulations. To
350 accomplish this, a constant water discharge and a constant sediment flux, in equilibrium
351 with the flow field, are defined at the upstream boundary, while a fixed water level is pro-
352 vided downstream. Flow and sediments are allowed to freely leave the system from the
353 downstream boundaries, thus, letting the bed to change in accordance with the hydro-
354 dynamics. The sediment transport is evaluated with the total-load closure of *Engelund*
355 *and Hansen* [1967], and sediment are assumed uniform with a diameter $d_s^* = 0.5\ mm$.
356 The transverse bed slope effects are accounted for in Delft3D by adopting the approach
357 of *Ikeda et al.* [1981]. Here the related parameter α_{bn} is set equal to 5, that corresponds
358 to a value of the *Talmon et al.* [1995] coefficient r equal to 0.88, well within the range
359 of the values suggested by *Bolla Pittaluga et al.* [2003]. The value emplyed represents
360 a good compromise between the value commonly used in the analytical analysis and the

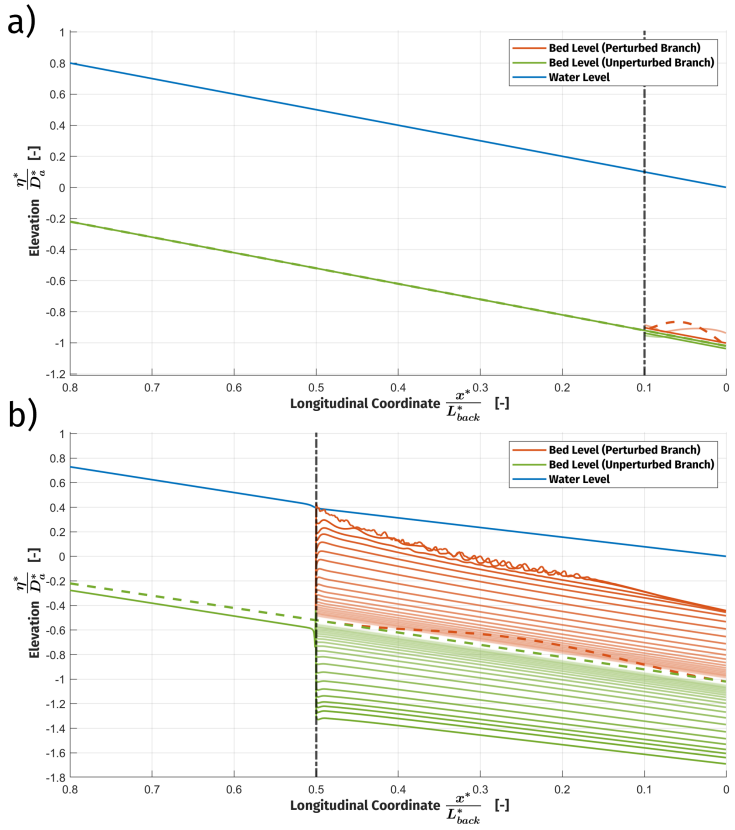

Figure 4. Bed profile evolution in numerical simulations. The figure illustrates the temporal evolution of the width-averaged bed profiles for two distinct branches, as derived from simulations. The branch experiencing the bed perturbation is visually represented in orange, while the other branch is delineated in green. The initial conditions for each channel are denoted by dashed lines. The blue line corresponds to the free-surface elevation. The black vertical line signifies the coordinate of the bifurcation node. The two panels depict the evolution of the same channel for $\beta = 16$, differing only in the length of the branches. Panel a) presents findings for the scenario with $L_b = 0.1$, wherein the perturbation traverses beyond the domain, leading to the system returning to its initial bed equilibrium. In contrast, panel b) showcases results for $L_b = 0.5$, demonstrating that the perturbed branch undergoes gradual deposition until reaching closure. Simultaneously, the alternate branch erodes over time to accommodate the heightened flow.

value often used in numerical simulations ($\alpha_{bn} = 10$) to avoid unrealistic channel incision (*Baar et al.* [2019]; *Iwantoro et al.* [2020]; *Van der Wegen and Roelvink* [2012]). Regarding the streamwise bed slope effects, the *Bagnold* [1966] approach is used with the default value of α_{bs} =1. As a design choice, the morphological acceleration factor *MorFac* is not utilized at the initial stages of the simulation to prevent inducing numerical artefacts at the bifurcation node where non-linearities may be present. However, once the system approaches the new equilibrium state, the morphological factor is set to values ranging from 10 to 100 to enhance the possible modest morphological variations in the system.

3.3 Results and Discussions

The linear stability analysis conducted for the symmetrical bifurcation of sand-bed rivers yields the algebraic relation (28) for the critical aspect ratio. In simple terms, β_{cr} serves as the demarcation point distinguishing configurations where the symmetrical solution remains stable (for β values less than β_{cr}) from configurations in which one of the two branches gains dominance (for β values greater than β_{cr}). Differently from the solution (29) of *Bolla Pittaluga et al.* [2015] hereafter referred to as BCK, the current theoretical framework establishes a direct correlation with the flow conditions at the node and the lengths of the branches L_b.

Our numerical simulations consistently reveal a small water level asymmetry between the two branches at the bifurcation node, in line with the findings of *Edmonds and Slingerland* [2008]. Consequently, it enforces the necessity of a more sophisticated nodal condition rather than relying on the assumption of constant water level as originally proposed by *Bolla Pittaluga et al.* [2003]. It is worth noting that the significance of this phenomenon diminishes as the branch lengthens, particularly for values surpassing the backwater length. Therefore, the solution proposed by *Bolla Pittaluga et al.* [2003] can be regarded as an asymptotic condition that the system would approach when the bifurcation is far enough from the downstream boundaries.

Consistently with the findings of *Bolla Pittaluga et al.* [2015], it has been observed that sand-bed and gravel-bed rivers exhibit contrasting behaviours as Shields values increase, as depicted in Figure 5. This disparity is attributed to the degree of non-linearity inherent in each sediment transport closure for varying Shields values. Additionally, the transverse sediment discharge plays a crucial role, with a more pronounced effect in rivers characterized by coarser grain sizes and, consequently, lower Shields values.

However, the present theory offers a novel insight, demonstrating that the reduction in the length of the branches exerts a stabilizing influence on the bifurcation evolution, resulting in more stable symmetrical configurations. Figure 5 visually illustrates the asymptotic behaviour of the original BCK model, wherein the neutral stability curve diverges for lower values of L_b. However, it is important to underline that the solution is still linearly dependent on the two parameters α and r introduced by *Bolla Pittaluga et al.* [2003]. The first is defined experimentally, but it still needs a careful determination for various configurations since it is a measure of the 2-D effects due to the bifurcation node. A first progress in this direction has been made by *Redolfi et al.* [2016], who linked the value of α with the wavelength of the steady damped alternate bars arising due to the instability mechanism originally found by *Zolezzi & Seminara* [2001]. Basically, the presence of the bifurcation exerts an upstream influence if the aspect ratio of the upstream channel is higher than the resonant value found by *Blondeaux & Seminara* [1985]. Recently, *Redolfi* [2023] further provided a physically-based estimation of the cell length assuming that the critical aspect ratio, for which the symmetric solution becomes unstable, should be equal to the resonant value as formulated by *Camporeale et al.* [2007]. As for the parameter r, it is expected to have an effect only on the bedload transport direction. Consequently, while employing a total load formulation akin to *Engelund and Hansen* [1967], it is important to recognize that the stabilizing effect of the transverse slope may be subject to some overestimation.

The numerical simulations confirm the increased stability observed in configurations featuring shorter branch lengths, as illustrated in Figure 6. In the numerical contest, we classify as stable (indicated by red dots) the cases where the initial perturbation leaves the domain without influencing the flow partitioning at the node. Conversely, instances where the perturbation increases in time, resulting in the dominance of one of the bifurcating branches, are labeled as unstable (marked by blue dots). Notably, there were only a few simulations where the final equilibrium of the system displayed a residual but steady discharge asymmetry (of the order of 2% in magnitude). These simula-

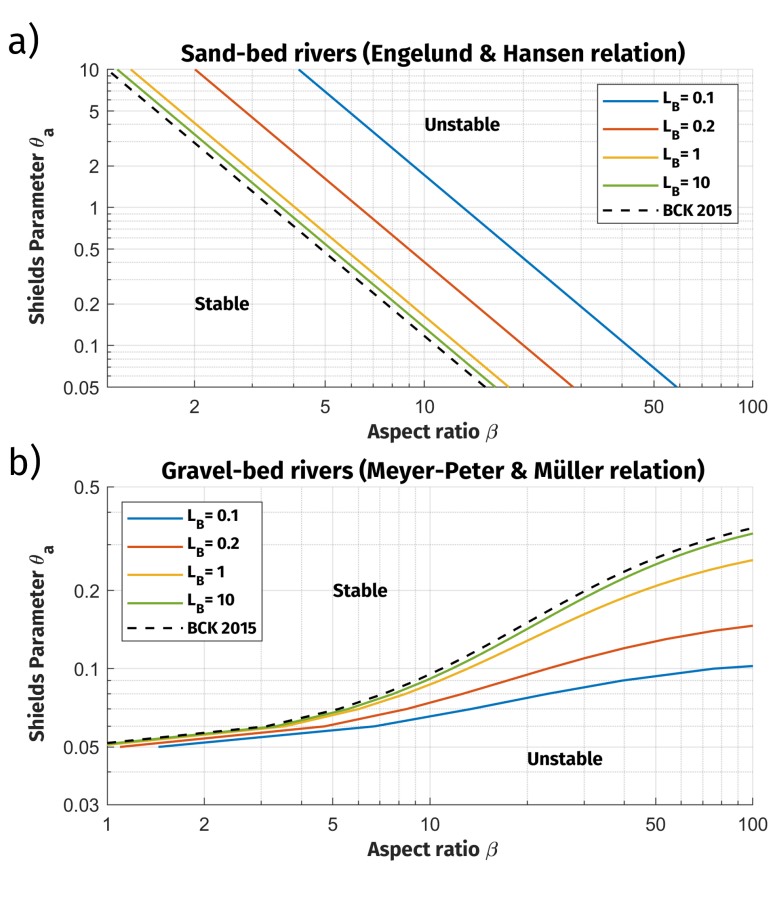

Figure 5. Opposite behaviour of gravel and sand bed rivers. Neutral stability curve of the symmetrical solution in the (β, ϑ_a) parameter space for different values of the dimensionless length L_b. Panel a) is representative of sand-bed rivers, where the *Engelund and Hansen* [1967] relation has been used. Panel b) shows the results using *Meyer-Peter and Müller* [1948] for gravel-bed rivers. In each section, the continuous lines show the present solution, while the staggered lines represent the BCK solution for the same set of parameters. Each line splits the graph into stable and unstable areas. (Parameters: $\alpha r = 1$, $Fr = 0.3$.)

tions, represented by green dots in Figure 6, are denoted as critical conditions due to their proximity to the critical value established by the theoretical framework. Furthermore, it is noteworthy how, in most instances, the configurations require longer times to reach the final equilibrium the closer the system is to the critical conditions.

The underlying mechanism entails that a small perturbation of the flow depth in the branch, could in turn affect the sediment transport capacity. When the carrying capacity of a branch exceeds the supply of sediments from upstream, that particular branch experiences overall erosion. Conversely, the other bifurcate undergoes a reduction of its ability to transport sediments downstream, consequently leading to sediment deposition. Over time, the gradual increase of the deposition may lead to the complete closure of the branch. Simultaneously, the remaining branch continues to erode until the riverbed establishes a renewed equilibrium in alignment with the altered flow discharge conditions. The closer is the system to the critical conditions, the smaller are the differences in carrying capacity, thus, requiring longer times to achieve an equilibrium.

Figure 6 clearly shows how the variation of the branches length alone is able to define stable/unstable configurations. For instance, fixing the aspect ratio β to 16 (i.e. keeping the upstream channel width equal), it is evident that merely extending the length of the branches L is sufficient to destabilize the system.

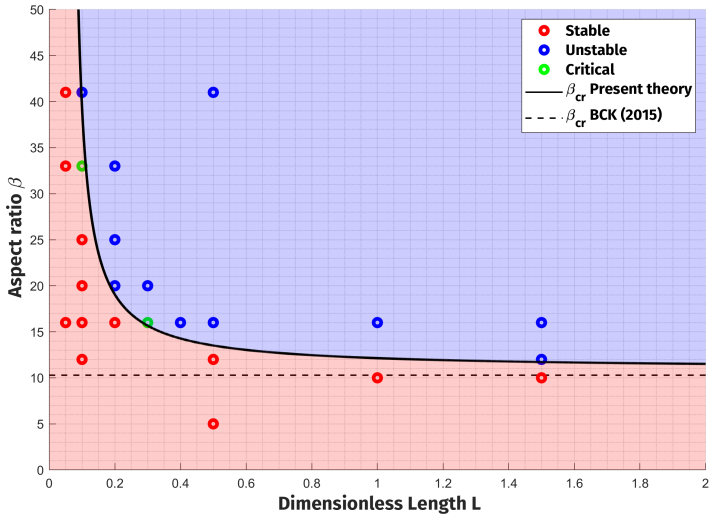

Figure 6. Stability of symmetrical river bifurcations. Neutral stability diagram of bifurcations with symmetrical downstream branches. The solid black line, denoting β_{cr} in the present study, highlights an area of heightened stability for diminishing dimensionless branch lengths, in comparison to the earlier work by BCK (depicted by the dashed line). The diagram is dichotomized by the β_{cr} line into regions of stable configurations (indicated by the red shading) and unstable configurations (indicated by the blue shading). The stable and unstable states, as determined through numerical simulations, are marked by coloured dots corresponding to the respective shading. Notably, the critical instances, signifying equilibrium with marginal stability accompanied by slight asymmetry, are represented by the green dots. (Parameters: $\alpha = 1.3$, $r = 0.88$, $\vartheta = 0.15$, $Fr = 0.31$.)

The equilibrium solutions resulting from the aforementioned concepts are determined by solving the non-linear system of equations derived from the nodal point conditions. For each aspect ratio of the main channel, denoted as β, we endeavor to identify multiple solutions within the system. These solutions encompass both the scenario of an equal partitioning of the flow and instances where one of the two branches carries a greater fraction of the flow.

The equilibrium solutions once again conform to the conventional pattern of a pitchfork bifurcation commonly observed in such configurations. In cases where β is low, the solitary solution corresponds to the equal partitioning of the flow between the branches. However, with an increase in β beyond the critical value β_{cr}, the symmetrical solution loses stability, resulting in a diversion of more flow toward one of the branches.

Figure 7 illustrates the equilibrium diagram for various values of the branch length, denoted as L_b. The solutions are depicted using the discharge asymmetry between the branches, as described in equation (31). The diagram clearly highlights the heightened stability of configurations for the smallest branch length. In contrast, an increase in L_b

brings the equilibrium diagram closer to the one obtained through the solution by BCK. Nonetheless, a slight disparity between the two solutions persists, which is attributed to the variations in flow conditions elucidated in equation (30). Once again, numerical sim-

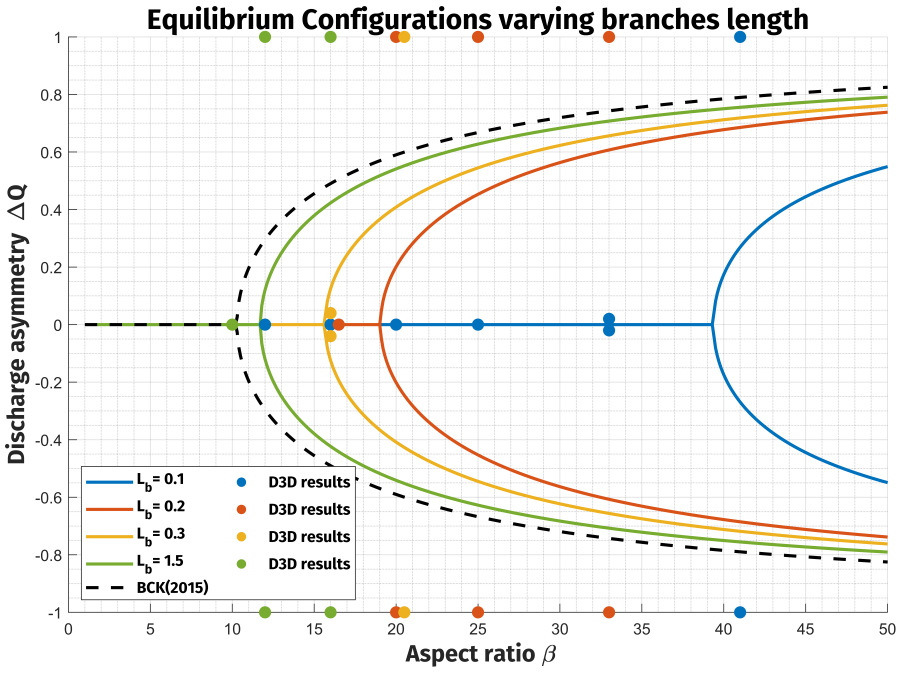

Figure 7. Equilibrium configurations of symmetrical river bifurcations. In this plot, each continuous line of a specific colour corresponds to a pitchfork bifurcation delineating the equilibrium diagram associated with a particular dimensionless length of the branches, denoted as L_b. The solutions are expressed in terms of discharge asymmetry between the branches ΔQ. The black dashed line is indicative of the BCK solution, in which the branch length is not accounted for. The dots presented on the graph signify the final equilibrium obtained from numerical simulations, aligned with the corresponding colour scheme of the lines. (Parameters: $\alpha = 1.3$, $r = 0.88$, $\vartheta = 0.15$, $Fr = 0.31$.)

ulations effectively discriminate between symmetrical configurations that exhibit stability and those that manifest instability accordingly to the present theory. However, in cases of unstable configurations, the final equilibrium assumes the form of the closure of the perturbed branch, leading to the complete diversion of flow toward the other branch (i.e., $\Delta Q = \pm 1$). This discrepancy with the analytical model can be attributed to its assumption of uniform flow within the branches. This assumption may be no longer valid when the perturbed branch undergoes sediment deposition, reaching a point at which it can no longer adapt its bed to accommodate the incoming sediments due to the reduced transport capacity. Notably, a recent study by *Barile et al.* [2023] extended the two-cell model to encompass partially avulsing bifurcations. Their findings once again highlight that as the downstream branches lengthen, the degree of asymmetry increases, potentially culminating in the complete avulsion of the system.

4 Asymmetrical Case

4.1 Results and Discussions

Encountering symmetrical bifurcations within a natural riverine setting proves to be a rarity, primarily due to the continuous evolutionary dynamics that typically drive these features towards pronounced asymmetry. Such conditions are commonly observed in both mountainous gravel-bed rivers and in low-lying sand-bed rivers reaching their downstream end in deltas. During field observations in mountainous braided networks, *Zolezzi et al.* [2006] reported that gravel-bed rivers tend to display highly unbalanced bifurcations, wherein the most carrying branch is generally wider and deeper. The effect of different branch widths is incorporated for in our analytical framework through the parameter denoted as r_b. Another prevalent occurrence is observed in meandering rivers, where the presence of cut-off channels gives rise to branches marked by significant disparities in both length and width (*Slingerland and Smith* [1998]). In the present investigation, these effects are accounted for through the parameters γ_L and r_b, contributing to a comprehensive understanding of the phenomenon. Furthermore, the aggregate width of downstream branches is frequently greater than that of the upstream channel, a characteristic represented here by the parameter r_a. *Edmonds and Slingerland* [2007] have measured, in several bifurcations within river-dominated deltas, an average downstream enlargement of the order of 1.7. Consequently, it becomes reasonable to postulate the presence of energy losses at the bifurcation node (through the coefficient ξ), arising from localized width variations or instances where the angle between the streamlines and the branches' thalweg deviates. Pertinently, a recent study related to confluences [*Ragno et al.*, 2021] has revealed the significant impact of downstream water level asymmetries on the stability of bifurcation confluence loops. Hence, our analysis incorporates this effect through the parameter Δh^L.

In this section, we investigate the influence of each one of the asymmetry parameters introduced above singularly. The objective of this analysis is to discern and isolate their respective impacts on the equilibrium configuration of bifurcations. Noteworthy, the following considerations are posed selecting a given value of the branches length. However, the previous results concerning the enhanced stability for shorter branch lengths still hold. Therefore, the following considerations will work to any value of L_b and the related β_{cr}. Within river bifurcations characterized by distinct branch lengths, the equal partitioning of the flow is rarely encountered. As the length ratio γ_L is augmented, it becomes evident that the shorter branch consistently accommodates a greater proportion of the flow. This is attributable to the advantageous influence of the free-surface slope that the shorter branch experiences relative to its longer counterpart, as depicted in Figure 8. Curiously, noteworthy arrangements arise in scenarios featuring elevated aspect ratios β, wherein the preeminence in conveying flow can shift to the longest branch. In such cases, any perturbation in the shorter branch affecting the carrying capacity might lead to an incipient flow diversion into the longest branch. Given the large upstream channel width, the stabilizing effect of the transverse slope is not able to counteract this tendency, thus, leading to the complete dominance of the longest branch.

A slope advantage has also been analyzed by *Redolfi et al.* [2019], who studied the combined effect of the slope advantage with the coexistence of upstream channel curvature. They found that the slope advantage can compensate for the effect of channel curvature under sub-resonant conditions. However, the length of the branches itself was not accounted for in their formulation, thus, possibly leading to less asymmetrical partitioning even for higher β.

Salter et al. [2018] investigated the effect of prograding branches finding an oscillating behaviour due to the restoring feedback of the milder slope in the longer branch. They also showed that shorter branches respond quicker to variation of sediment supply, thus, showing lower asymmetric partitioning.

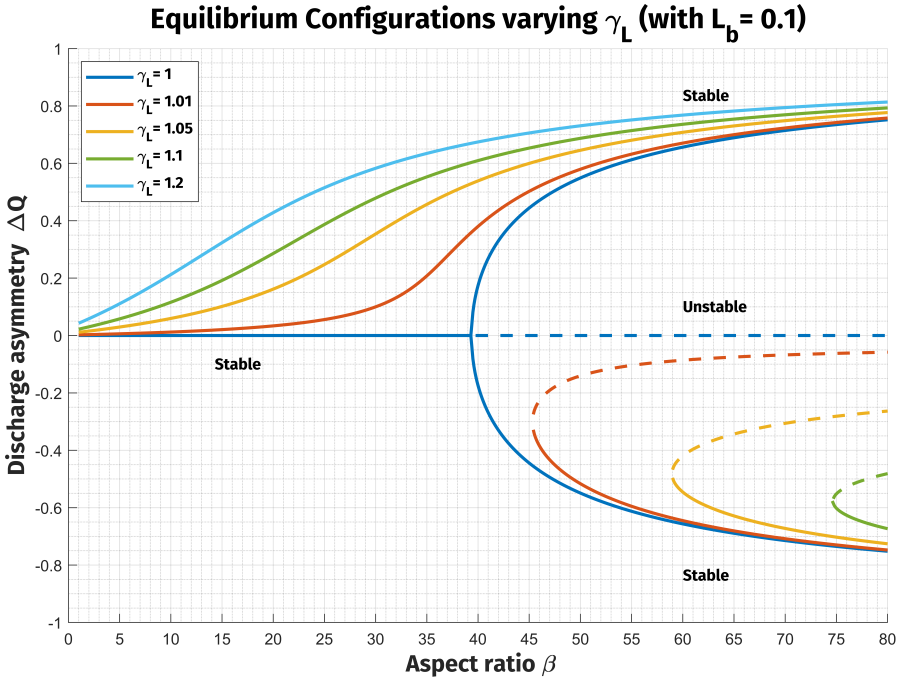

Figure 8. Equilibrium configurations of bifurcations with different branch lengths. The equilibrium diagram, delineated in relation to discharge asymmetry, illustrates the modulation of flow distribution concerning alterations in the length ratio, denoted as γ_L. Each continuous line, distinguished by a specific hue, represents stable solutions, while the dashed curve denotes instances where the symmetrical solution becomes unstable. (Parameters: $\alpha = 1.3$, $r = 0.88$, $\vartheta = 0.15$, $Fr = 0.31$.)

Figure 9 illustrates the influence of varying branch widths on the flow distribution within bifurcations. The blue line in the graph corresponds to the case in which branch widths are equal (i.e., $r_b = 0.5$), resulting in an even partition of the flow for configurations below β_{cr}. Notably, increasing the branch width ratio, the flow distribution varies accordingly diverting a larger proportion of the flow towards the wider branch. In those configurations, the largest branch is inevitably dominant and would easily move toward the closure of the narrow branch for high aspect ratios. However, it is essential to recognize that in our computation, the branches can solely adjust their bed levels, with their widths considered as fixed parameters. In contrast, field observations indicate that such asymmetrical distribution often arises from adaptations in channel width in response to incoming flow conditions. To account for this effect, we can refer to the local approach by *Miori et al.* [2006] where they relaxed the assumption of fixed-banks, but assuming that downstream effects do not influence the bifurcation. Figure 10 describes the effect of varying the aggregated widths within the branches in relation to the upstream channel width. Evidently, an elevation in the ratio r_a, signifying an enlargement downstream, results in a decreased number of configurations where the symmetric solution is stable. On the other hand, narrower branches correspondingly lead to an augmentation of the critical aspect ratio β_{cr}. In those configurations, the flow is expected to increase its velocity entering the branches, thereby enhancing their conveyance capacity. As a consequence, any perturbation in the system can be flushed away preserving the unobstructed flow in both branches. Conversely, when a localized widening occurs at the bifurcation node, the flow decelerates, creating favourable conditions for sediment deposition within

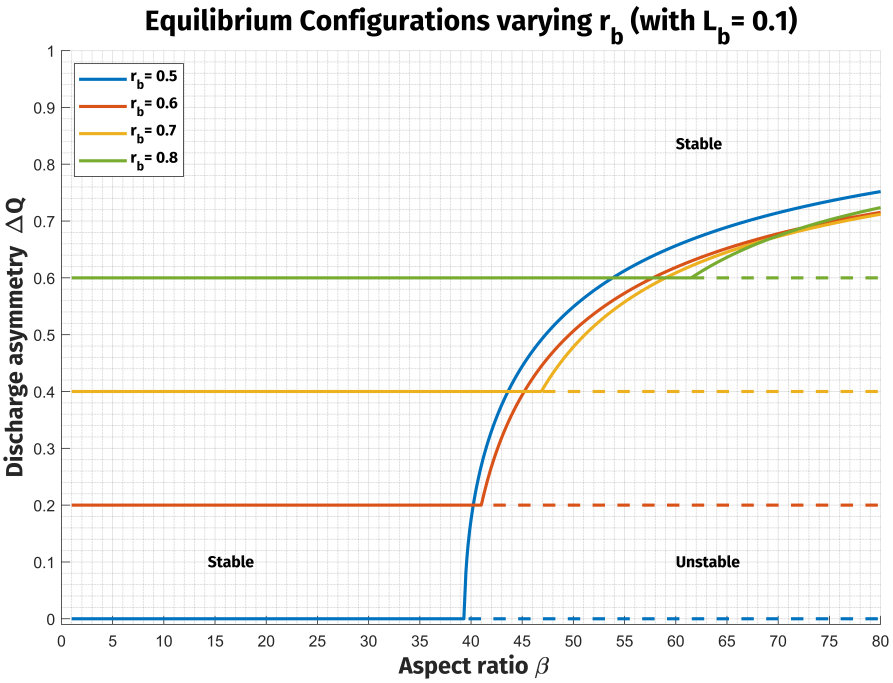

Figure 9. Equilibrium configurations of bifurcations with different branch widths. The equilibrium diagram, delineated in relation to discharge asymmetry, illustrates the modulation of flow distribution concerning alterations in the branch width ratio, denoted as r_b. Each continuous line, distinguished by a specific hue, represents stable solutions, while the dashed curve denotes instances where the symmetrical solution becomes unstable. (Parameters: $\alpha = 1.3$, $r = 0.88$, $\vartheta = 0.15$, $Fr = 0.31$.)

the branches. In accordance with the rationale underlying pressurized flows, it is reasonable to attribute localized head losses to local width variations or bifurcation angles between the branches. The extent of this influence on the critical aspect ratio β_{cr} is contingent upon the value of ξ, which is an order-one parameter. Figure 11 provides a visual representation of how alterations in ξ can impact the equilibrium configurations. The findings indicate that enhancing dissipations leads to a more stabilized system due to the consequent increase in water level disparities at the bifurcation, thereby amplifying the differences in free-surface slopes between branches. This impact is discernible in equation (16), where $\Delta h^L = 0$ and $\gamma_L = 1$: an increase in ξ accentuates the importance of kinetic head differences, thereby increasing the slope variations for branches of equal length L_b.

In Figure 12, an examination of distinct downstream water levels is compared with the symmetric case ($\Delta h^L = 0$) depicted in blue. Notably, variations in the downstream water level introduce a free surface slope advantage within one branch, consequently inducing an acceleration in flow velocity. This increase in flow speed, in turn, amplifies the branch's capacity for carrying flow. Consequently, under circumstances marked by elevated aspect ratios, the branch can attain dominance. However, it is worth mentioning that instances might arise wherein perturbations affecting the favoured channel could still destabilize the system, causing a redirection of flow toward the opposite branch.

Nevertheless, the parameter Δh^L is formulated without accounting for the adjustment of the downstream free surface based on flow conditions. In the realm of natural

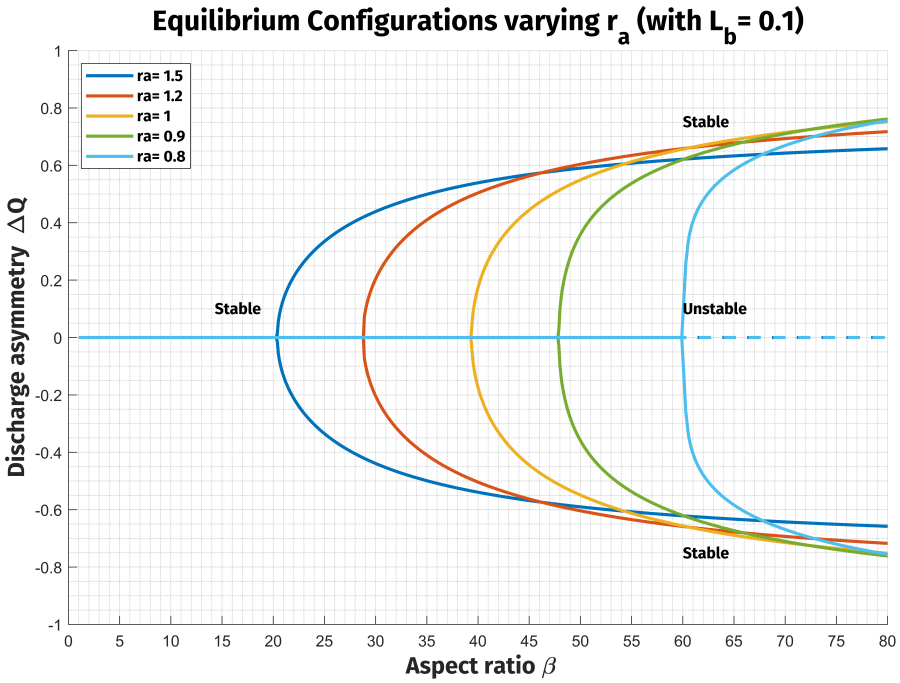

559 **Figure 10. Equilibrium configurations of bifurcations with downstream enlarge-**
560 **ment.** The equilibrium diagram, delineated in relation to discharge asymmetry, illustrates the
561 modulation of flow distribution concerning alterations in the ratio between the aggregate of the
562 branch widths and the upstream channel width, denoted as r_a. Each continuous line, distin-
563 guished by a specific hue, represents stable solutions, while the dashed curve denotes instances
564 where the symmetrical solution becomes unstable. (Parameters: $\alpha = 1.3$, $r = 0.88$, $\vartheta = 0.15$,
565 $Fr = 0.31$.)

621 environments over extended temporal scales, such fixed definitions of water levels are scarcely
622 encountered. More commonly, the configurations of interest, particularly those with shorter
623 branch lengths, manifest in bifurcation-confluence loops. In the context of confluences,
624 a direct correlation between water level asymmetry and the square of the Froude num-
625 ber has been established, underscoring the inevitability of water level adaptations in re-
626 sponse to flow conditions. In this regard, *Ragno et al.* [2021] succeeded in coupling a con-
627 fluence model with the work of *Bolla Pittaluga et al.* [2003], thereby accommodating down-
628 stream flow fluctuations. Their findings indicate that confluences tend to elevate the wa-
629 ter level within the branch responsible for carrying the greater flow rate. This dynamic
630 prompts a reduction in the slope of the dominant branch, creating a negative feedback
631 mechanism that strives to restore equilibrium in the distribution of water and sediment
632 fluxes.

633 5 Conclusions

634 The current study has introduced a revision of the well-established two-cell model
635 originally proposed by *Bolla Pittaluga et al.* [2003] for the purpose of predicting the sta-
636 bility of river bifurcations. The model is based on the foundational assumption of main-
637 taining constant water levels between the branches at the bifurcation node. However,
638 it is evident that this assumption no longer holds true in scenarios where downstream
639 conditions significantly impact the distribution of flow at the bifurcation node. Through

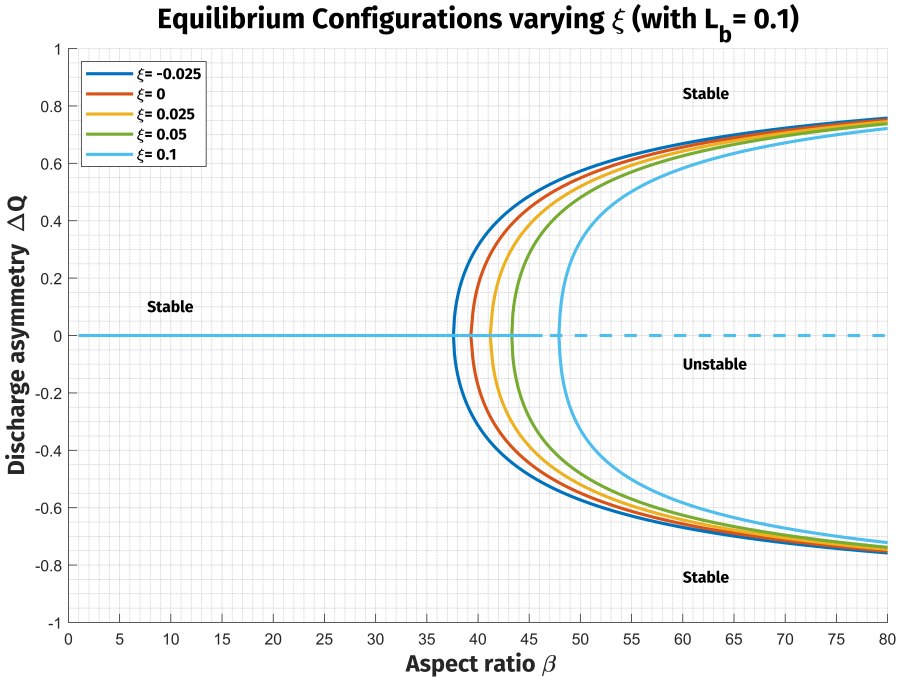

Figure 11. Equilibrium configurations of bifurcations with localized kinetic head losses. The equilibrium diagram, delineated in relation to discharge asymmetry, illustrates the modulation of flow distribution concerning alterations in the differences between kinetic losses of the branches, denoted with the parameter $\Delta\xi$. Each continuous line, distinguished by a specific hue, represents stable solutions, while the dashed curve denotes instances where the symmetrical solution becomes unstable. (Parameters: $\alpha = 1.3$, $r = 0.88$, $\vartheta = 0.15$, $Fr = 0.31$.)

numerical simulations, it has been observed that any alteration to the bed of the branching channels leads to corresponding adjustments in the uniform flow depth profile. These adjustments, driven by downstream boundary conditions, consequently result in discernible changes to the water surface elevation at the bifurcation node. Especially noteworthy is the effect of branch length on this phenomenon. In cases where the branching channels are of limited length, the aforementioned alterations in flow division become non-trivial, causing an asymmetry that contributes to the stabilization of the bifurcation system. Conversely, when the branching channels exhibit substantial length, the impact of these alterations diminishes, allowing the original model to remain a reliable predictor. Thus, to accommodate these intricate effects within analytical models, a formulation akin to an energy balance at the bifurcation node has been seamlessly integrated into the model of *Bolla Pittaluga et al.* [2003].

The newly introduced theory clearly demonstrates that symmetrical bifurcations attain enhanced stability as the length of the branches decreases, as substantiated by numerical simulations. Nonetheless, truly symmetrical systems are a rarity in natural settings, prompting the inclusion of various asymmetry-inducing elements in the theory. Intriguingly, when considering branches of differing lengths, the shorter branch emerges as the preferred path for flow distribution. Nevertheless, scenarios may arise, particularly in the context of large rivers characterized by substantial aspect ratios, where the longer branch may dominate by capturing the majority of the upstream flow.

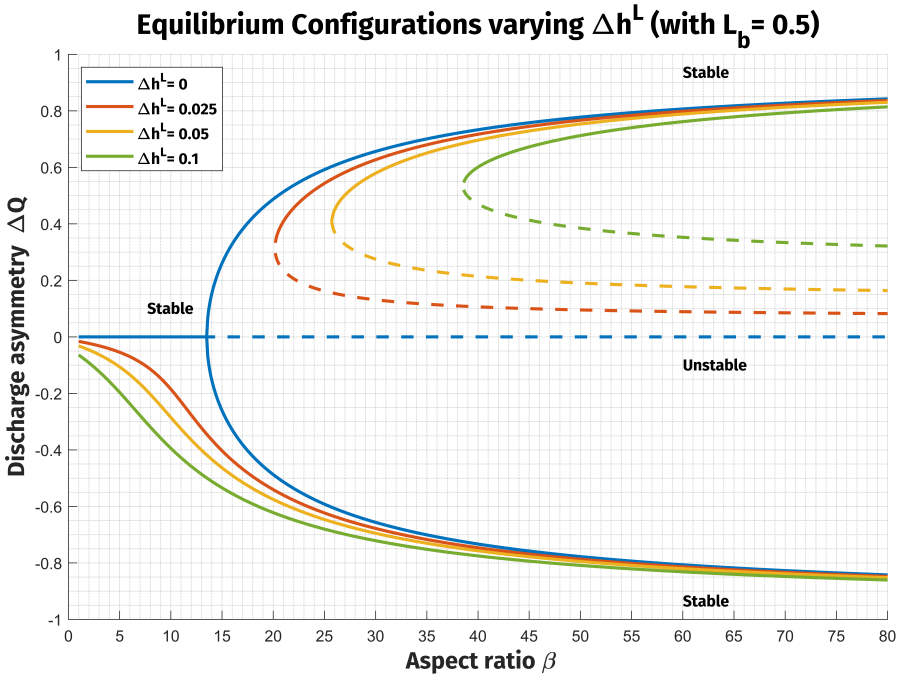

Figure 12. Equilibrium configurations of bifurcations with downstream water level asymmetry. The equilibrium diagram, delineated in relation to discharge asymmetry, illustrates the modulation of flow distribution concerning alterations in the water level asymmetry downstream, denoted with the parameter Δh^L. Each continuous line, distinguished by a specific hue, represents stable solutions, while the dashed curve denotes instances where the symmetrical solution becomes unstable. (Parameters: $\alpha = 1.3$, $r = 0.88$, $\vartheta = 0.15$, $Fr = 0.31$.)

However, some limitations within the framework presented herein need to be acknowledged, although they might be of straightforward incorporation. Factors such as channel curvature and its influence on sediment partitioning between branches, widening of the channels, and the presence of free/forced bars or prograding delta branches have not been included within the current model.

In light of these considerations, it is plausible to anticipate that the novel model presented in this study will facilitate an enhanced understanding of bifurcation evolution in estuarine environments subject to tidal fluctuations.

Acknowledgments

The authors declare that they have no conflict of interest. This paper has been supported by the Italian Ministerial grant PRIN 2022 “Allogenic and Autogenic controls of DElta MOrphodynamics (AADEMO)”, n. 2022P9Z7NP - CUP C53D23002080006, by the Po River Basin Authority grant ”Updating the Po River Management Programme and integration with the delta branches” - CUP F22G16000000001, and by the Italian Ministerial grant PRIN 2022 “Reconciling coastal flooding protection and morphological conservation of shallow coastal environments (Prot&Cons)”, n. 2022FZNH82 - CUP C53D23002050006.

References

Baar, A. W., Boechat Albernaz, M., Van Dijk, W. M., & Kleinhans, M. G. (2019), Critical dependence of morphodynamic models of fluvial and tidal systems on empirical downslope sediment transport, *Nature Communications, 10(1)*, 4903.

Bagnold, R. A. (1966), An approach to the sediment transport problem from general physics, *US government printing office*.

Barile, G., Redolfi, M., & Tubino, M. (2023). Analysis of autogenic bifurcation processes resulting in river avulsion, *EGUsphere, 2023, 1-26*.

Bertoldi, W. and M. Tubino (2007), River bifurcations: Experimental observations on equilibrium configurations, *Water Resources Research, 43*, 10, DOI: 10.1029/2007WR005907.

Bertoldi, W., Zanoni, L., Miori, S., Repetto, R., and Tubino, M. (2009). Interaction between migrating bars and bifurcations in gravel bed rivers. *Water Resources Research, 45(6)*.

Blondeaux, P., and Seminara, G. (1985), A unified bar–bend theory of river meanders, *Journal of Fluid Mechanics, 157*, 449-470.

Bolla Pittaluga, M., Repetto, R. and M. Tubino (2003), Channel bifurcation in braided rivers: Equilibrium configurations and stability, *Water Resources Research, 39(3)*, 1046, doi:10.1029/2001WR001112.

Bolla Pittaluga, M., Luchi, R. and G. Seminara (2014), On the equilibrium profile of river beds, *J. Geophys. Res. - Earth, 119*, 317–332, doi: 10.1002/2013JF002806.

Bolla Pittaluga, M., G. Coco, and M. G. Kleinhans (2015), A unified framework for stability of channel bifurcations in gravel and sand fluvial systems, *Geophys. Res. Lett., 42*, doi:10.1002/2015GL065175.

Camporeale, C., Perona, P., Porporato, A., & Ridolfi, L. (2007). Hierarchy of models for meandering rivers and related morphodynamic processes. *Reviews of Geophysics, 45(1)*.

Colombini, M., Seminara, G., and Tubino, M. (1987), Finite-amplitude alternate bars, *Journal of Fluid Mechanics, 181, 213-232*.

Edmonds, D. A. and R. L. Slingerland (2007), Mechanics of river mouth bar formation: Implications for the morphodynamics of delta distributary networks, *Journal of Geophysical Research: Earth Surface, 112(F2)*.

Edmonds, D. A. and R. L. Slingerland (2008), Stability of delta distributary networks and their bifurcations, *Water Resources Research, 44*, W09426, doi:10.1029/2008WR006992.

Engelund, F. and E. Hansen (1967), A monograph on sediment transport, *Technical University of Denmark, Technisk Forlag*, Copenhagen, Denmark.

Ikeda, S., Parker G. and K. Sawai (1981), Bend theory of river meanders. Part 1 - Linear development, *J. Fluid Mech., 112*, 363–377.

Iwantoro, A. P., Van Der Vegt, M., and Kleinhans, M. G. (2020), Morphological evolution of bifurcations in tide-influenced deltas, *Earth Surface Dynamics, 8(2)*, 413–429.

Jerolmack, D. J. (2009), Conceptual framework for assessing the response of delta channel networks to Holocene sea level rise. *Quaternary Science Reviews, 28(17)*, 1786—1800.

Kleinhans, M. G., Jagers, H. R. A., Mosselman, E. and C. J. Sloff (2008), Bifurcation dynamics and avulsion duration in meandering rivers by one-dimensional and three-dimensional models, *Water Resources Research, 44*, W085454, doi:10-1029/2007WR005912.

Leonardi, N., Kolker, A. S., & Fagherazzi, S. (2015). Interplay between river discharge and tides in a delta distributary. *Advances in Water Resources, 80*, 69-78.

Lesser, G. R., Roelvink, J. V., van Kester, J. T. M., and Stelling, G. S. (2004), Development and validation of a three-dimensional morphological model. *Coastal*

Engineering, 51(8-9), 883-915.

Meyer-Peter, E. and R. Müller (1948), Formulas for bedload transport, *III Conf. of Internat. Ass. of Hydraul. Res., Stockholm, Sweden.*

Miori, S., Repetto, R. and M. Tubino (2006), A one-dimensional model of bifurcations in gravel bed channels with erodible banks, *Water Resources Research, 42*, W11413, doi:10.1029/2006WR004863.

Nienhuis, J. H., Ashton, A. D., Edmonds, D. A., Hoitink, A. J. F., Kettner, A. J., Rowland, J. C., and Törnqvist, T. E. (2020). Global-scale human impact on delta morphology has led to net land area gain. *Nature, 577(7791)*, 514—518.

Ragno, N., Tambroni, N., and Bolla Pittaluga, M. (2020), Effect of small tidal fluctuations on the stability and equilibrium configurations of bifurcations, *Journal of Geophysical Research: Earth Surface, 125(8)*, e2020JF005584.

Ragno, N., Redolfi, M., and Tubino, M (2021), Coupled morphodynamics of river bifurcations and confluences, *Water Resources Research, 57*, e2020WR028515. https://doi.org/10.1029/2020WR028515

Ragno, N., Redolfi, M., Tambroni, N., and Tubino, M (2023), Modelling steady grain sorting in river bifurcations, *Journal of Geophysical Research: Earth Surface*, e2023JF007230.

Redolfi, M., Zolezzi, G., and Tubino, M. (2016), Free instability of channel bifurcations and morphodynamic influence, *Journal of Fluid Mechanics, 799*, 476-504.

Redolfi, M., Zolezzi, G., and Tubino, M. (2019), Free and forced morphodynamics of river bifurcations, *Earth Surface Processes and Landforms, 44(4)*, 973-987.

Redolfi, M. (2023). Defining the length parameter in river bifurcation models: a theoretical approach. *Earth Surf. Process. Landforms. 2023;48:2121–2132.*

Salter, G., Paola, C., & Voller, V. R. (2018). Control of delta avulsion by downstream sediment sinks. *Journal of Geophysical Research: Earth Surface, 123, 142–166.* https://doi.org/10.1002/2017JF004350

Seminara, G. (2006). Meanders. *Journal of Fluid Mechanics, 554*, 271–297. doi:10.1017/S0022112006008925

Slingerland, R. and N. D. Smith (1998), Necessary condition for a meandering-river avulsion, *Geology, 26 (5)*, 435–438.

Van der Wegen, M., & Roelvink, J. A. (2012), Reproduction of estuarine bathymetry by means of a process-based model: Western Scheldt case study, the Netherlands, *Geomorphology, 179*, 152-167.

van Rijn, L. C. (1984), Sediment transport, II, Suspended load transport, *J. Hydraul. Eng., 110(11)*, 1431–1456.

Viero, D.P., Dubon, S.L. and Lanzoni, S. (2018). Chute cutoffs in meandering rivers: formative mechanisms and hydrodynamic forcing. In Fluvial Meanders and Their Sedimentary Products in the Rock Record (eds M. Ghinassi, L. Colombera, N.P. Mountney, A.J.H. Reesink and M. Bateman). https://doi.org/10.1002/9781119424437.ch8

Talmon, A. M., Struiksma, N., and Van Mierlo, M. C. L. M. (1995), Laboratory measurements of the direction of sediment transport on transverse alluvial-bed slopes, *J. Hydraul. Res., 33 (4)*, 495–517.

Tejedor, A., Longjas, A., Edmonds, D. A., Zaliapin, I., Georgiou, T. T., Rinaldo, A., and Foufoula-Georgiou, E. (2017). Entropy and optimality in river deltas. *Proceedings of the National Academy of Sciences, 114(44)*, 11651–11656.

Wang, Z. B., Fokkink, R. J., De Vries, M. and A. Langerak (1995), Stability of river bifurcations in 1D morphodynamics models, *J. Hydraul. Res., 33 (6)*, 739–750.

Wilkerson, G. V., and Parker, G. (2011), Physical basis for quasi-universal relationships describing bankfull hydraulic geometry of sand-bed rivers, *J. Hydraul. Eng., 137(7)*, 739–753.

Williams, G.P. (1978), Bank-Full discharge of rivers, *Water Resources Research* 14(6): 1141–1154.

Wolman, M.G. and J.P. Miller (1960), Magnitude and frequency of forces in geomorphic processes, *Journal of Geology* 68: 54–74.

Zolezzi, G. and Seminara, G. (2001), Downstream and upstream influence in river meandering. Part 1. General theory and application to overdeepening, *Journal of Fluid Mechanics, 438(13)*, 183–211.

Zolezzi, G., Bertoldi, W., Tubino, M., Smith, G. H. S., Best, J. L., Bristow, C. S., & Petts, G. E. (2006). Morphological analysis and prediction of river bifurcations, *Braided rivers: process, deposits, ecology and management, 36, 233–256.*

A: Coefficients of the asymmetrical linear system

The system of equations (14)-(17) is solved through a linearization procedure, in terms of the four unknowns [q_b, q_c, D_b, D_c]. With a perturbative approach, every variables and unknowns are expanded in terms of a small parameter δ as follows:

$$f = f_0 + \delta f_1 + \mathcal{O}(\delta^2) \ . \tag{A.1}$$

where f_0 represents the basic state and f_1 derives from a Taylor expansion around the basic state.

Substituting the expansions in the equations, it is possible to solve the system at each order of approximation. At the leading order, a set of non-linear algebraic equations in terms of the basic state variable arise, that can be solved with a central finite-difference solver.

The order δ problem consists of the homogeneous linear system of equations 20. The coefficients A_{ij} are defined as follows:

$$A_{11} = r_b, \tag{A.2}$$

$$A_{12} = r_c, \tag{A.3}$$

$$A_{13} = 0, \tag{A.4}$$

$$A_{14} = 0, \tag{A.5}$$

$$A_{21} = \frac{2 r_b \phi_{b0} \Phi_{\vartheta b}}{\phi_a q_{b0}}, \tag{A.6}$$

$$A_{22} = \frac{2 r_c \phi_{c0} \Phi_{\vartheta c}}{\phi_a q_{c0}}, \tag{A.7}$$

$$A_{23} = \frac{r_b \phi_{b0}}{\phi_a} \left(-2\Phi_{\vartheta b} C_{Db} - \frac{2\Phi_{\vartheta b}}{D_{b0}} + \phi_{nb} \right), \tag{A.8}$$

$$A_{24} = \frac{r_c \phi_{c0}}{\phi_a} \left(-2\Phi_{\vartheta c} C_{Dc} - \frac{2\Phi_{\vartheta c}}{D_{c0}} + \phi_{nc} \right), \tag{A.9}$$

$$A_{31} = \frac{2RL_b C_a^2 q_{b0}}{r_a r_b D_{b0}^3 C_{b0}^2} - 1 + \frac{2\phi_{b0}\Phi_{\vartheta b}}{\phi_a q_{b0}}, \tag{A.10}$$

$$A_{32} = \frac{2RL_b \gamma_L C_a^2 q_{c0}}{r_a r_b D_{c0}^3 C_{c0}^2}, \tag{A.11}$$

$$\begin{aligned} A_{33} = &- \frac{R}{r_a r_b} \left[1 + \frac{C_a^2 q_{b0}^2 L_b}{D_{b0}^3 C_{b0}^2} \left(2C_{Db} + \frac{3}{D_{b0}} \right) \right] + \\ &- \frac{\phi_{b0}}{\phi_a} \left(2\Phi_{\vartheta b} C_{Db} + 2\frac{\Phi_{\vartheta b}}{D_{b0}} - \phi_{nb} \right), \end{aligned} \tag{A.12}$$

$$A_{34} = \frac{R}{r_a r_b}\left[1 + \frac{C_a^2 q_{c0}^2 L_b \gamma_L}{D_{c0}^3 C_{c0}^2}\left(2C_{Dc} + \frac{3}{D_{c0}}\right)\right], \tag{A.13}$$

$$A_{41} = \frac{2L_b C_a^2 q_{b0}}{D_{b0}^3 C_{b0}^2} + (1+\xi)\frac{Fr^2 q_{b0}}{D_{b0}^2}, \tag{A.14}$$

$$A_{42} = -\frac{2L_b \gamma_L C_a^2 q_{c0}}{D_{c0}^3 C_{c0}^2} - (1+\xi)\frac{Fr^2 q_{c0}}{D_{c0}^2}, \tag{A.15}$$

$$A_{43} = -\frac{C_a^2 L_b q_{b0}^2}{D_{b0}^3 C_{b0}^2}\left(2C_{Db} + \frac{3}{D_{b0}}\right) - (1+\xi)\frac{Fr^2 q_{b0}^2}{D_{b0}^3}, \tag{A.16}$$

$$A_{44} = \frac{C_a^2 L_b \gamma_L q_{c0}^2}{D_{c0}^3 C_{c0}^2}\left(2C_{Dc} + \frac{3}{D_{c0}}\right) + (1+\xi)\frac{Fr^2 q_{c0}^2}{D_{c0}^3}, \tag{A.17}$$

where:

$$\Phi_{\vartheta b} = \frac{m\vartheta_{b0}}{\vartheta_{b0} - \vartheta_{cr}}, \tag{A.18}$$

$$\Phi_{\vartheta c} = \frac{m\vartheta_{c0}}{\vartheta_{c0} - \vartheta_{cr}}, \tag{A.19}$$

$$C_{Db} = \frac{1}{C_{b0}}\left.\frac{\partial C_b}{\partial D_b}\right|_{D_{b0}}, \tag{A.20}$$

$$C_{Dc} = \frac{1}{C_{c0}}\left.\frac{\partial C_c}{\partial D_c}\right|_{D_{c0}}, \tag{A.21}$$

$$\phi_{nb} = \frac{1}{n(D_{b0})}\left.\frac{\partial n}{\partial D_b}\right|_{D_{b0}}, \tag{A.22}$$

$$\phi_{nc} = \frac{1}{n(D_{c0})}\left.\frac{\partial n}{\partial D_c}\right|_{D_{c0}}, \tag{A.23}$$

$$R = \frac{\alpha r}{\beta_a \sqrt{\vartheta_a}}. \tag{A.24}$$

Noteworthy, for the case of symmetrical bifurcations, the coefficients (A.18)-(A.23) are equal between b and c. Therefore, they can be summed up as in (23).